applied sciences

MDPI

Article

Study of Thermal Effect in the Interaction of Nanosecond Capillary Discharge Extreme Ultraviolet Laser with Copper

Huaiyu Cui [1,2], Yongpeng Zhao [1,*], Muhammad Usman Khan [1], Dongdi Zhao [1] and Zhigang Fan [2]

[1] National Key Laboratory of Science and Technology on Tunable Laser, Harbin Institute of Technology, Harbin 150001, China; cuihuaiyu_hit@163.com (H.C.); usmanphy138@yahoo.com (M.U.K.); 13603602080@163.com (D.Z.)

[2] Research Center for Space Optics Engineering, Harbin Institute of Technology, Harbin 150001, China; fzg@hit.edu.cn

* Correspondence: zhaoyp3@hit.edu.cn

Received: 21 November 2019; Accepted: 24 December 2019; Published: 26 December 2019

Abstract: Interaction of Extreme Ultraviolet (EUV) laser with matters is an attractive subject since novel phenomena always occur under the effect of high energy photons. In this paper, the thermal effect involved in the interaction of a capillary discharge 46.9 nm laser with copper was studied theoretically and experimentally. The temperature variation of the laser-irradiated region of copper was calculated. According to the results, the copper surface was ablated obviously and presented the trace of melting, evaporation, and resolidification, which suggested the thermal effect occurred on the surface during the laser irradiation.

Keywords: 46.9 nm laser; copper; thermal effect; laser-induced damage

1. Introduction

With the development of modern science and technology, there is an urgent need in developing new techniques for micro- and nano-processing of various materials in order to create small features in large areas at high speed. Until now, various methods were explored to break the diffraction limitation, such as metalenses, e.g., Hence, micro/nanostructures were created in the interaction of laser with solid targets. For example, during the interaction of the laser with matters, nanoparticles could be formed with luminescent or plasmonic properties [1–3], especially copper plasmonic nanoparticles [4]. Among all the methods for creating small scale structures on various surfaces by lasers, decreasing the laser wavelength is still the most direct way [5,6]. Due to the high photon energy, the damage mechanism of the extreme ultraviolet (EUV) to X-rays differs dramatically from the damage induced by longer-wavelength light, such as ultraviolet/visible/infrared light. Therefore, a novel phenomenon always occurs in the interaction of shot-wavelength light with matters. For instance, Thanh-Hung Dinh et al. created sub-nanometer craters on the surface of a silicon substrate by controlling strong excitations induced by a single femtosecond extreme ultraviolet pulse from a SACLA free-electron laser [7].

Generally, the thermal effect decreases the resolution of laser-processing. Capillary discharge EUV laser, because of its suitable wavelength and nanosecond duration, could be used as a proper radiation source in the study of thermal effect in the interaction process of the laser at a short wavelength with materials. After the capillary discharge EUV laser was demonstrated [8], scientists began to study the interaction of this nanosecond EUV laser with various materials. Due to the characteristic of the laser duration and the photon energy, the corresponding damage mechanism is complex including thermal and non-thermal effects. Rocca's group studied the damage threshold and damage mechanism

of Sc/Si multilayer mirrors exposed to a capillary discharge 46.9 nm laser, the thermal nature of the damage mechanism was presented [9]. Later, the group optimized a 2D hydrodynamic code, PULLUX, by adding new absorption and atomic physics, which enabled the simulation of the ablative properties of EUV and X-ray lasers. According to the analysis, over 85% of the ablation occurs within the first half of the laser pulse and lateral heat transport dominates at later times increasing the surface feature size future [10].

The big difference of damage mechanisms and characteristics between EUV ablation and longer-wavelength lasers ablation always present in molecular solids, because EUV photon carries enough energy to break any chemical bond in an irradiated material [11]. In this interaction process, the non-thermal effect always occurs initially and makes a major contribution to the ablation. However, for the interaction of XUV/SXR with metals which carries ample free electrons under room temperature, the ablation results may indicate a different interaction process and damage mechanism. The research on the thermal effect in the interaction of nanosecond EUV laser with metals will help to understand the damage mechanism of these short wavelength radiation sources. There are rare reports focusing on the thermal effect and melting trace in the damage induced by a 46.9 nm laser since the high photon energy is supposed to be the key role to trigger the damage on materials. In our previous work, different targets were measured by a nanosecond capillary discharge a 46.9 nm laser and melting trace was observed on copper [12,13]. In this paper, ablation induced by a 46.9 nm laser on copper was further researched. The thermal effect and non-thermal effect in the interaction process were discussed. The results indicated that the nanosecond EUV laser could trigger drastic surface behavior (i.e., phase explosion) at quite a low fluence with the contribution of thermal effect, which is generally supposed to be less crucial than non-thermal effect. Since the interaction of nanosecond EUV laser with matters is complex and hard to model accurately, the research on thermal effect by EUV laser could help to understand the damage mechanism of EUV laser further.

2. Materials and Methods

In the experiment, the radiation source was a nanosecond capillary discharge EUV laser operating at a 46.9 nm with a pulse width of 1.7 ns. The laser was produced using Ne-like Ar plasma excited with a fast current pulse [14,15]. The laser was focused into a distorted shape by a toroidal mirror at a grazing incidence angle of 7°. The target was located on a 2D stage to be irradiated at different positions of the surface and beam axis. An X-ray diode (XRD) was used to measure the relative energy of the laser. The target we used in the experiment was copper with a polished surface. The roughness of the surface was estimated to be less than 100 nm. To avoid the formation of an oxide layer on the copper surface, the targets were preserved carefully and moved into the vacuum chamber as quickly as possible. At the beginning of the irradiation, XRD was moved into the beam path to measure the laser energy. After the laser output was stable, the target was moved in and the irradiation started. The surface of the copper target was irradiated by multiple pulses of focused a 46.9 nm laser at different positions along the beam axis. After the irradiation, the damaged surface was detected by SEM (Scanning Electron Microscope).

COMSOL Multiphysics (COMSOL Inc, Stockholm, Sweden), which is based on the finite element algorithm (FEM), was used in this section to calculate the temperature variation of copper in and after the laser irradiation. Since the attenuation length for copper at 46.9 nm is approximately 10 nm [16], the material is very nearly opaque to a 46.9 nm laser. In the simulation, the laser was treated as a surface heat source. The energy of the beam was assumed to be absorbed over a negligibly small distance into the material relative to the size of the object that was irradiated. The simulation was built in the module of 'Heat Transfer in Solids'.

Since the critical electron density of a 46.9 nm laser is typically higher than solid, the laser could penetrate the expanding plasma plume and continue to heat the target surface directly throughoutthe duration of the laser pulse. Therefore, the heat source term should be involved in the calculation until the pulse ended. To build the function to describe the focused beam, spatial and temporal distribution

of the laser was analyzed. Figure 1 showed the Gaussian fitting of normalized temporal distribution. The full width at half maximum (FWHM) of pulse duration was 1.6 ns. The spatial distribution of the laser was complex since the laser was focused on grazing incidence which caused the optical aberration. Even though, mostly the laser energy was focused into a small area that could be fitted into a Gaussian shape. Approximately, the spatial distribution of the focused laser was simulated as a Gaussian distribution. The function of describing the focused laser spot was as follow:

$$P_{in}(x, y, t) = P_0 \exp\left[-A\left(\frac{t-\tau}{\tau}\right)^2\right] \exp\left[-\frac{(x-x_0)^2}{2r^2} - \frac{(y-y_0)^2}{2r^2}\right] \quad (1)$$

where P_0 was the peak power of the laser, A was the Gaussian parameter for a temporal profile, τ was the FWHM of pulse duration and r was the beam radius.

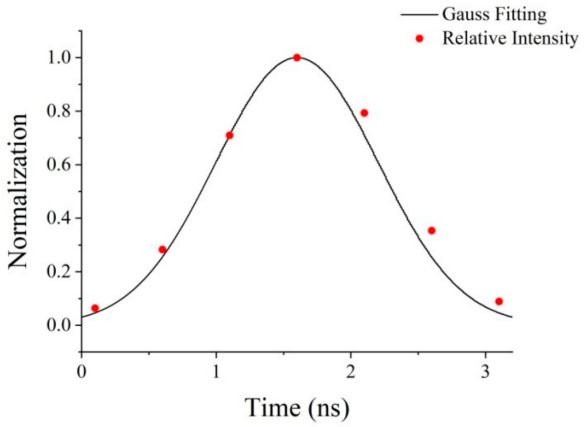

Figure 1. Gaussian fitting of the normalized temporal distribution of a 46.9 nm laser.

The calculated field was built to be a cylinder with a radius of 1 mm and a height of 0.5 mm, of which the volume was much smaller than the copper target used in the experiment. It was aimed at reducing the amount of calculation while, at the same time, ensuring accuracy. The surface of the sample was set to be heat-insulated to the surrounding environment since the interaction occurred in the vacuum chamber with pressure below 10^{-4} Pa. The simulation was built under the condition that the whole pulse energy of the laser with the peak power P_0 of 6×10^4 W was contributed to raising the temperature of the surface (in the experiment, the laser with ~50 μJ and ~100 μJ were both used to irradiate Cu targets. In both cases, the melting trace was detected. According to the detection, in the case of 100 μJ, the evaporation of the surface was more intense. In the simulation, the laser with the energy of 100 μJ was chosen to be calculated). According to the calculation, the temperature variation of the central point of the irradiated surface at 0–5 ns was simulated and showed in Figure 2. The point reached the peak temperature of 3900 K at 2.1 ns after the laser began to heat the surface. The temperature of the target mostly depended on the effect of the laser heating and the thermal diffusion in the volume. Before 2.1 ns, laser heating occupied a dominant position resulting in the fast rise of the temperature. Then, after the transient balance at 2.1 ns, the temperature was mostly affected by the thermal diffusion. After 3.2 ns, at the end of the laser pulse, the temperature was still mostly determined by the thermal diffusion effect. It was worth noting that the peak temperature of the central point far exceeded the melting point and evaporating point of copper. Therefore, the irradiated surface would be melted and evaporated by the laser irradiation.

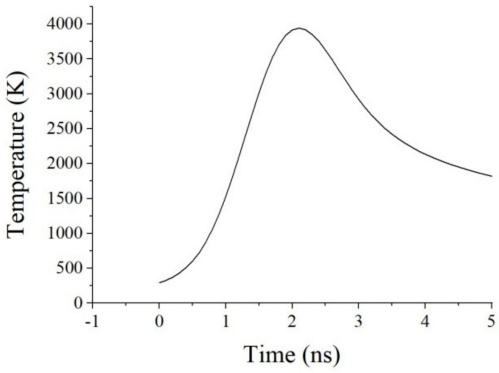

Figure 2. Temporal temperature variation of the center point on the sample surface at 0–5 ns.

Figure 3 showed the temperature distribution of a 1D copper surface at 2.1 ns processed by Gaussian fitting. The diameter of the area going through the temperature rise was 580 μm. The diameter of the area under the temperature beyond the melting point of copper was 197 μm, under the temperature beyond the evaporating point was 89 μm. According to the Global definition, the beam radius was set to be 100 μm. The result above showed an obvious thermal diffusion at the surface, which due to the good heat-conducting property of copper.

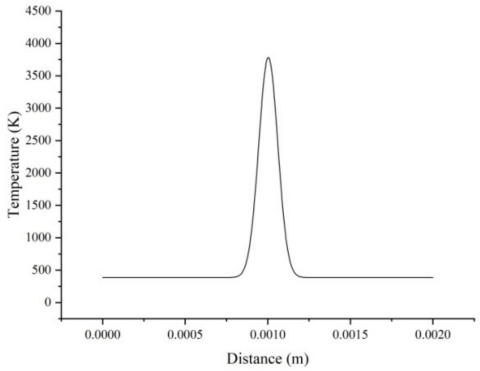

Figure 3. Temperature distribution of the target surface at 2.1 ns.

The temperature variation on the depth of the sample along the center axis was simulated and showed in Figure 4. The laser energy was delivered into the volume and caused the temperature to rise. With the depth increasing, the peak temperature of the corresponding point was decreasing. When it reached 20 μm, there was almost no temperature rise. The size of the sample was much larger than the beam radius and heat penetration depth. Therefore, the temperature rise of the whole sample induced by laser heating could be neglected. Based on that, we could expect that there was no temperature accumulation to the whole sample by multiple pulses of laser irradiation.

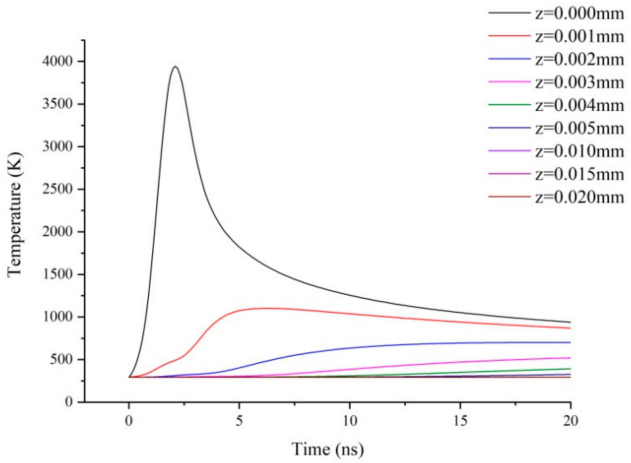

Figure 4. Temperature variation on the different depth of the sample along the center axis.

3. Results and Discussion

After the irradiation of the focused 46.9 nm laser with multiple pulses, ablation patterns shown in Figure 5 were detected by SEM. The ablation pattern induced by single-pulse was also detected, which indicated the laser fluence was above the damage threshold of copper. The melting occurred at a similar area of the ablation patterns and became more obvious with the increasing of the pulse number. The melting area was measured to be 770 μm^2, 420 μm^2, 270 μm^2 and 120 μm^2, with respect to the pulse number of 6, 3, 2 and 1. In the experiment, the interval time between every two pulses was longer than 30 s to avoid the superposition of the surface relaxation. The following laser pulse irradiated the surface was already melted by the last laser pulse. The increasing melting area with the added pulse number indicated that the characteristic of the melted surface was changed to promote the heat diffusion. Therefore, in the case of multiple laser pulses, the damaged area was melted again and again and presented quite a drastic surface behavior. From Figure 5, the melting part was only a small area in the whole damaged area. In most parts of the damage, the fluence of the laser was not high enough to trigger evident melting or evaporation behavior on the copper surface. However, the irradiation of the laser modified the surface into a different condition presenting a contrast with the color of the unabated area under SEM detection.

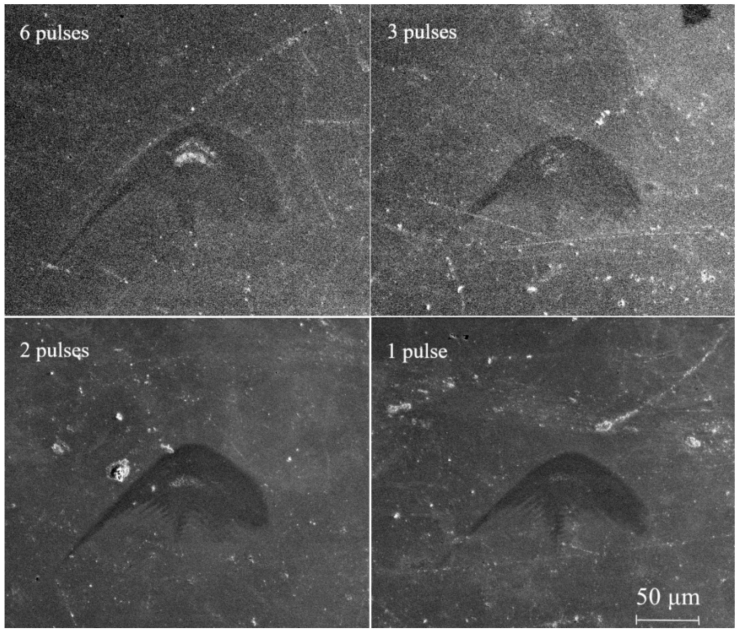

Figure 5. Whole view of the ablation patterns on copper-induced by multiple laser pulses.

To study the difference between the damaged and undamaged areas, the edge of the damaged area was detected and shown in Figure 6. The fringes at the top of the damaged area were induced by the inhomogeneous energy distribution of the original laser spot and the diffraction effect occurred in the transmission. In the undamaged area, scratches induced by the surface polishing were observed clearly. Nonetheless, they did not exist in the damaged area, which proved the laser cleaning effect.

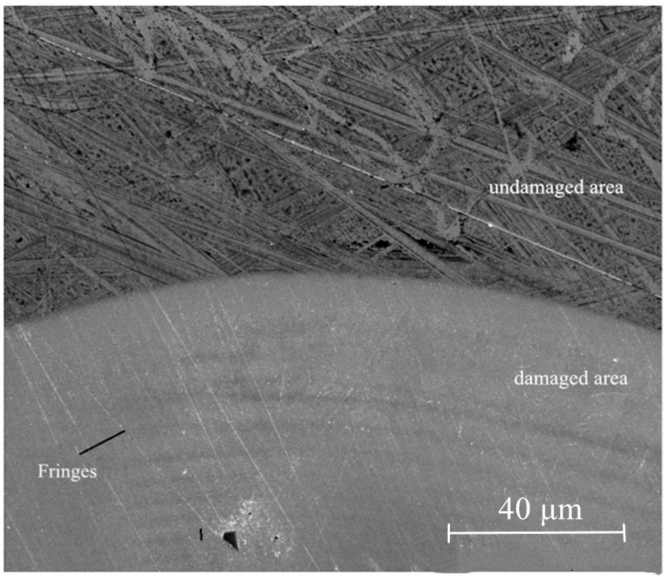

Figure 6. Details at the edge of the damaged area.

To analyze the melting under different laser fluence, the focused laser spot at a different distance from the focus point was studied in Figure 7. We calculated the average fluence by the function as below:

$$F = E_{pulse} / S_{damaged} \quad (2)$$

where E_{pulse} was the pulse energy and $S_{damaged}$ was the area of the damaged pattern. It was worth noting that $S_{damaged}$ was measured on the damaged surface of polymethyl methacrylate (PMMA), not copper, since PMMA was more sensitive to the irradiation of the 46.9 nm laser and would help to present the whole shape of the focused 46.9 nm laser. Figure 8 showed the measurement of the damaged area on PMMA. The pattern was the whole view of the one showed at the right image in Figure 7. The damage pattern was detected by White light interferometer (WLI). The area was measured to be 0.04 mm^2. With the estimated energy of 100 μJ, the average fluence of the laser was calculated to be 250 mJ/cm^2. Figure 9a,b referred to the whole view of the patterns at left and in the middle of Figure 7. The area was measured to be 0.1 mm^2 and 0.06 mm^2, corresponding to the fluence of 100 mJ/cm^2 and 160 mJ/cm^2. The focused laser spot was caught by a Ce-doped Yttrium Aluminum Garnet (Ce: YAG) scintillator with the transformation from the invisible laser into visible light. The real shape of the focused laser at a different distance from the focus spot was presented in the middle row of Figure 7. The first row in the picture was the contour map obtained from the intensity of the visible spot. The color bar showed the scale of the relative intensity of the spot. The intensity of the laser spot and transformed visible spot were not in a linear relationship. However, the intensity distribution of the visible spot indicated the general condition of the intensity distribution of the focused laser spot. The third row was the corresponding damage pattern at each position. The white lines circled the melting position. To compare the three rows, the shape of the laser spot and the damage pattern were coincident. In each position, the melting occurred at the position under the laser irradiation with a higher intensity, which indicated a higher fluence.

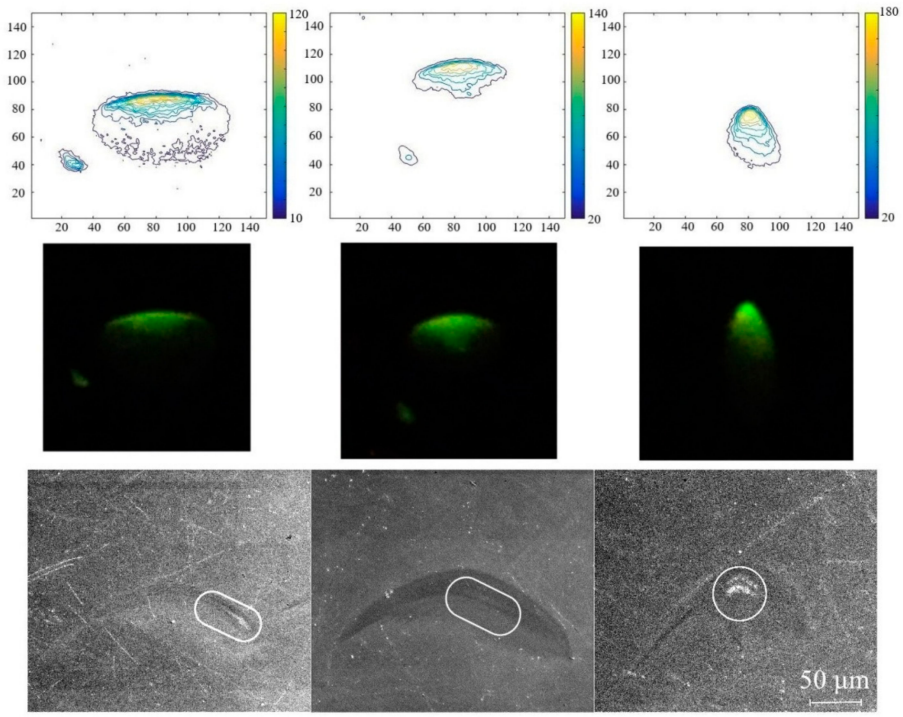

Figure 7. Melting trace under different laser fluences.

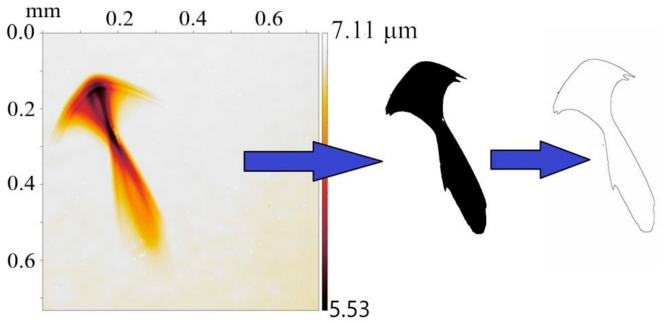

Figure 8. Measurement of the damaged area on PMMA.

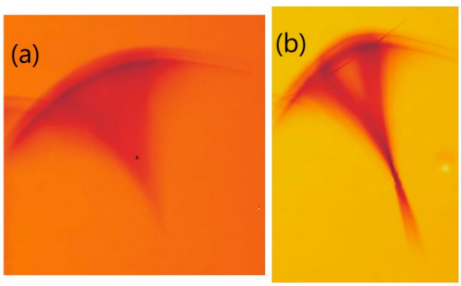

Figure 9. Whole image of the patterns at other positions: (**a**) Position at left of the patterns in Figure 7; (**b**) Position in the middle of the patterns in Figure 7.

In the damaged area, the melting traces shown in Figure 10 were expressed in several kinds of morphologies. The surface absorbed the laser energy, then was melted or evaporated and resolidified into nanoparticles, as shown in Figure 10a. Before cooled into a solid phase, the particles might converge and then be resolidified into small bulk, as shown in Figure 10b. Since the target was located vertical to the beam path and nearly vertical to the horizontal plane, most of the nanoparticles were drop-down because of gravity. Since the plasma expansion occurred near the surface of the target, there are still some particles left on the surface, which showed strong evidence that the surface behavior was

drastic due to the irradiation of the laser. Phase explosion would occur during the interaction. Based on that, the thermal effect was strongly involved in the interaction. In future research, the mica sheet would be used below the target to catch the nanoparticles ejected from the surface to study the size distribution. In the ablation area, it was also found a large melting area around the impurities inset the copper surface, as shown in Figure 11. It was supposed to be caused by the heat accumulation around the interface of the impurity and copper. That would be another evidence to prove the thermal effect in the damage.

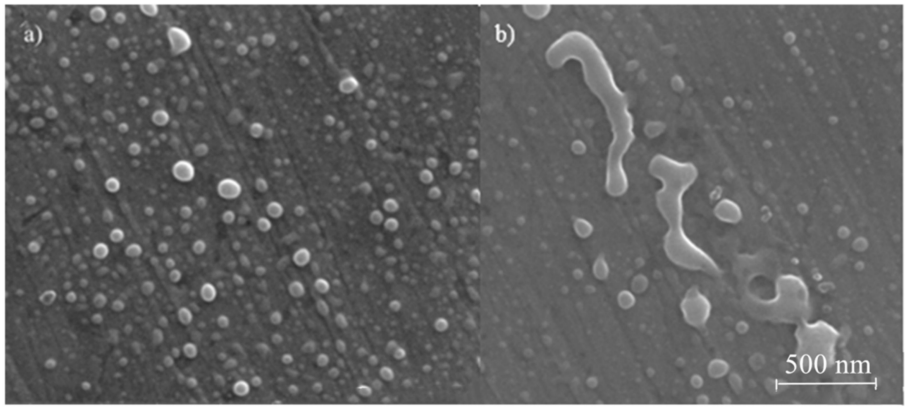

Figure 10. Different types of melting traces: (**a**) Nanoparticles; (**b**) Melted bulk.

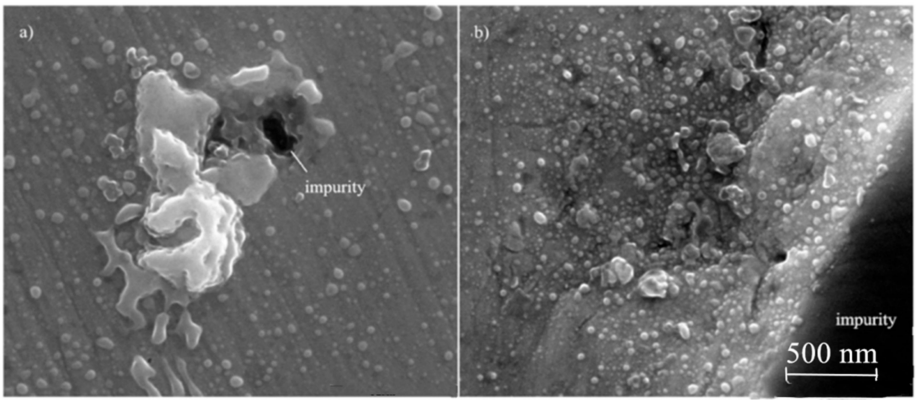

Figure 11. Large area melted around the impurity: (**a**) Melting area around the impurity; (**b**) Boundary line between impurity and copper.

Melting trace was detected in the ablation area induced by both single and multiple pulses of laser irradiation. Figure 12 showed the melted surface induced by 25, 12, 6, 3, 2, and 1 pulse of laser irradiation. The area showed in Figure 12 was part of the whole damage area which presented the level of the melting. The melting behavior got more and more intense with the increasing number of laser pulses. When the pulse number was above 3, the surface evaporation was quite clear. According to the analysis, there was no temperature accumulation in the multiple pulses of laser irradiation. Therefore, we could expect that there was also evaporation occurred in single pulse irradiation, which was too faint to be detected clearly under SEM. The estimated average fluence of a 46.9 nm laser that could cause evaporation was much lower than the fluence of optical lasers that could cause surface evaporation of copper [17]. It is generally known that the damage threshold of EUV laser is much lower than that of the laser with a longer wavelength, which due to the contribution of the photon with quite a high energy. However, the melting or evaporation threshold of the same material is more related to the fluence of the light, not the photon energy. Therefore, we supposed the quite low evaporation threshold of a 46.9 nm laser indicated that the high photon energy of a 46.9 nm laser promoted the

thermal effect in the interaction process. More corresponding research is expected in the future to study the relationship between the high photon energy and the thermal effect.

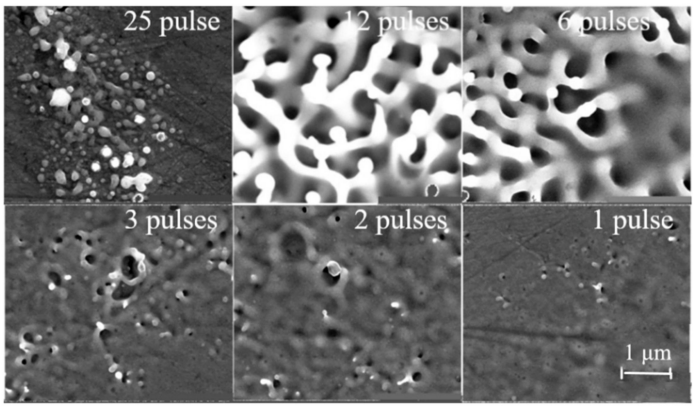

Figure 12. Melting and evaporation trace induced by multiple pulses of laser.

In the interaction of XUV laser radiation with solid targets, the damage could be classified into 'desorption' and 'ablation' [18]. If the local fluence of the laser is around the damage threshold, desorption is dynamically possible. Generally, a characteristic microscopic time scale for desorption varies from 200 fs to 3 ps [19]. However, in the case of the metallic surface, the dissipation of initial electronic or vibrational excitations from absorbed photons occurs on a time scale of a few femtoseconds. That means desorption cannot take place on a pure metallic surface. In addition, from the detection results, the surface behavior of copper-induced by the 46.9 nm laser irradiation was quite drastic, which fitted the 'ablation' expression better. Therefore, in the interaction of a 46.9 nm laser with copper, the damage on the target surface could be characterized as 'ablation'.

Copper contained plenty of free electrons under room temperature. That meant, in the interaction, the laser energy could be absorbed directly by free electrons, resulting in the temperature rise in the irradiated area. Then the lattices were distorted and the damage took place. In this process, the thermal effect was dominant. We could expect that most of the laser energy contributed to the temperature rise of the irradiated area. According to the simulation result, with the absorption of one pulse energy, the highest temperature of the irradiated area was above the evaporating point of copper. Therefore, the surface of copper was melted and evaporated by the irradiation of the 46.9 nm laser. According to the results, the surface behavior induced by a 46.9 nm laser on copper differed from that on other types of materials, such as large bandgap dielectrics (PMMA [20], BaF_2 [12]) and multiple layers [9]. In the case of dielectrics, regardless of the type of organic or inorganic, the damage always induced by a non-thermal effect, leaving clear patterns with a certain depth and a clean edge. The bound electrons absorb photon energy and are ionized. Or the molecular bond is directly broken by the photon. In the case of multiple layers, discoloration was detected resulting from heat-triggered interdiffusion in upper layers. Cracks covered damaged area indicated tensile stress induced by thermal expansion and the following cooling down process. The similar cracks were not observed in the damage of copper in this work because the material characteristic of copper is different from the multiple layers and also the fluence of the laser was lower which was not able to generate such a temperature difference. According to Reference [20], in the interaction of a 46.9 nm laser with solid targets, attenuation length was a crucial factor in determinate the damage mechanism, which was classified involving the traveling ionization wave of ablation and ablation threshold. Based on that statement, the damage that occurred on copper fits the former mechanism.

4. Conclusions

To sum up, the interaction of a 46.9 nm laser with copper was studied theoretically and experimentally. The ablation results showed an obvious thermal effect involved in the interaction

process, which presented melting and evaporation traces in the ablation area. It coincided with the calculation results. The fluence of the 46.9 nm laser that could cause the evaporation on the copper surface was much lower than that of optical lasers, which indicated the high photon energy promoted the thermal effect that occurred in the interaction process. This phenomenon is worth studying in the future to help understand the interaction of high energy photons with solid targets.

Author Contributions: Investigation, H.C.; Funding acquisition, Y.Z.; Resources, M.U.K.; Software, D.Z.; Supervision, Z.F. All authors have read and agreed to the published version of the manuscript.

Funding: This research was funded by the National Natural Science Foundation of China (NSFC), grant number 61875045.

Conflicts of Interest: The authors declare no conflict of interest. The funders had no role in the design of the study; in the collection, analyses, or interpretation of data; in the writing of the manuscript, or in the decision to publish the results.

References

1. Intartaglia, R.; Bagga, K.; Scotto, M.; Diaspro, A.; Brandi, F. Luminescent silicon nanoparticles prepared by ultra short pulsed laser ablation in liquid for imaging app lications. *Opt. Mater. Express* **2012**, *2*, 510–518. [CrossRef]
2. Hou, S.; Birowosuto, M.D.; Umar, S.; Anicet, M.A.; Tay, R.Y.; Coquet, P.; Tay, B.K.; Wang, H.; Teo, E.H.T. Localized Emission from Laser-Irradiated Defects in Two-Dimensional Hexagonal Boron Nitride. *2D Mater.* **2017**, *5*. [CrossRef]
3. Saleem, U.; Birowosuto, M.; Hou, S.; Maurice, A.; Kang, T.B.; Teo, E.H.T.; Tchernycheva, M.; Gogneau, N.; Wang, H. Light emission from localised point defects induced in GaN crystal by a femtosecond-pulsed laser. *Opt. Mater. Express* **2018**, *8*, 2703–2712. [CrossRef]
4. Desario, P.A.; Pietron, J.J.; Brintlinger, T.H.; McEntee, M.; Parker, J.F.; Baturina, O.; Stroud, R.M.; Rolison, D.R. Oxidation-stable plasmonic copper nanoparticles in photocatalytic TiO_2 nanoarchitectures. *Nanoscale* **2017**, *9*, 11720–11729. [CrossRef] [PubMed]
5. Cohen, A.E.; Soltis, S.M.; González, A.; Aguila, L.; Alonso-Mori, R.; Barnes, C.O.; Baxter, E.L.; Brehmer, W.; Brewster, A.S.; Brunger, A.T.; et al. Goniometer-based femtosecond crystallography with X-ray free electron lasers. *Proc. Natl. Acad. Sci. USA* **2014**, *111*, 17122–17127. [CrossRef] [PubMed]
6. Rath, A.D.; Timneanu, N.; Maia, F.R.N.C.; Bielecki, J.; Fleckenstein, H.; Iwan, B.; Svenda, M.; Hasse, D.; Carlsson, G.; Westphal, D.; et al. Explosion dynamics of sucrose nanospheres monitored by time of flight spectrometry and coherent diffractive imaging at the split-and-delay beam line of the FLASH soft x-ray laser. *Opt. Express* **2014**, *22*, 28914–28925. [CrossRef] [PubMed]
7. Dinh, T.H.; Medvedev, N.; Ishino, M.; Kitamura, T.; Hasegawa, N.; Otobe, T.; Higashiguchi, T.; Sakaue, K.; Washio, M.; Hatano, T.; et al. Controlled strong excitation of silicon as a step towards processing materials at sub-nanometer precision. *Commun. Phys.* **2019**, *2*, 150. [CrossRef]
8. Rocca, J.J.; Shlyaptsev, V.V.; Tomasel, F.G.; Cortázar, O.D.; Hartshorn, D.; Chilla, J.L. Demonstration of a discharge pumped table-top soft-x-ray laser. *Phys. Rev. Lett.* **1994**, *75*, 1236. [CrossRef]
9. Grisha, M.M.; Vaschenko, G.; Menoni, C.S.; Rocca, J.J. Damage to extreme ultraviolet Sc/Si multilayer mirrors exposed to intense 46.9nm-laser pulses. *Opt. Lett.* **2004**, *29*, 620–622. [CrossRef] [PubMed]
10. Rossall, A.K.; Aslanyan, V.; Tallents, G.J.; Kuznetsov, I.; Rocca, J.J.; Menoni, C.S. Ablation of Submicrometer Holes Using an Extreme-Ultraviolet Laser. *Phys. Rev. Appl.* **2015**, *3*, 064013. [CrossRef]
11. Liberatore, C.; Mann, K.; Müller, M.; Pina, L.; Juha, L.; Vyšín, L.; Rocca, J.J.; Endo, A.; Mocek, T. Short-wavelength ablation of polymers in the high-fluence regime. *Phys. Scr.* **2014**, *T161*, 014066. [CrossRef]
12. Zhao, Y.; Cui, H.; Zhang, S.; Zhang, W.; Li, W. Formation of nanostructures induced by capillary-discharge soft X-ray laser on BaF_2 surfaces. *Appl. Surf. Sci.* **2016**, *396*, 1201–1205. [CrossRef]
13. Zhao, Y.; Cui, H.; Zhang, W.; Li, W.; Jiang, S.; Li, L. Si and Cu ablation with a 46.9-nm laser focused by a toroidal mirror. *Opt. Express* **2015**, *23*, 14126–14134. [CrossRef] [PubMed]
14. Zhao, Y.; Mo, M.; Xie, Y.; Yang, S.; Wang, Q. Observation of a saturated soft X-raylaser in a low current capillary discharge. In Proceedings of the Conference on Lasers and Electro-Optics/Pacific Rim, Optical Society of America 2009, Shanghai, China, 30 July–3 August 2009.

15. Zhao, Y.; Jiang, S.; Xie, Y.; Yang, D.; Teng, S.; Chen, D.; Wang, Q. Demonstration ofsoft x-ray laser of Ne-like Ar at 69.8 nm pumped by capillary discharge. *Opt. Lett.* **2011**, *36*, 3458–3460. [CrossRef] [PubMed]
16. Chantler, C.T. Theoretical Form Factor, Attenuation, and Scattering Tabulation for Z = 1−92 from E = 1−10 eV to E = 0.4−1.0 MeV. *J. Phys. Chem. Ref. Data* **1995**, *24*, 71–643. [CrossRef]
17. Jordan, R.; Cole, D.; Lunney, J.G.; Mackay, K.; Givord, D. Pulsed laser ablation of copper. *Appl. Surf. Sci.* **1995**, *86*, 24–28. [CrossRef]
18. Kolacek, K.; Schmidt, J.; Straus, J.; Mackay, K.; Givord, D. Interaction of extreme ultraviolet laser radiation with solid surface: Ablation, desorption, nanostructuring. In Proceedings of the XX International Symposium on High Power Laser Systems and Applications, Chengdu, China, 25 August 2014; International Society for Optics and Photonics: Washington, DC, USA, 2015.
19. Doerr, D. *Laser Ablation and Desorption*; Experimental Methods in the Physical Sciences; Miller, J.C., Haglund, R.F., Eds.; Academic Press: Cambridge, MA, USA, 1997; Volume 30.
20. Tallents, G.J.; Wilson, S.A.; Lolley, J.; Aslanyan, V.; West, A.; Rossall, A.K.; Solis-Meza, E.; Wagenaars, E.; Menoni, C.S.; Rocca, J.J. Extreme ultraviolet laser ablation of solid targets. In Proceedings of the SPIE Optical Engineering + Applications, San Diego, CA, USA, 9 September 2019.